9-10-2012

Particulate optical scattering coefficients along an Atlantic Meridional Transect

G. Dall'Olmo
Plymouth Marine Laboratory

E. Boss
University of Maine, emmanuel.boss@maine.edu

M. J. Behrenfeld
Oregon State University

T. K. Westberry
Oregon State University

Particulate optical scattering coefficients along an Atlantic Meridional Transect

G. Dall'Olmo,[1,*] E. Boss,[2], M.J. Behrenfeld,[3] and T.K. Westberry[3]

[1]*Plymouth Marine Laboratory, Prospect Place, Plymouth, PL1 3DH, UK*
[2]*University of Maine, Orono, ME, 04469, USA*
[3]*Oregon State University, Corvallis, OR, 97331, USA*
[*]*gdal@pml.ac.uk*

Abstract: The particulate optical backscattering coefficient (b_{bp}) is a fundamental optical property that allows monitoring of marine suspended particles both in situ and from space. Backscattering measurements in the open ocean are still scarce, however, especially in oligotrophic regions. Consequently, uncertainties remain in b_{bp} parameterizations as well as in satellite estimates of b_{bp}. In an effort to reduce these uncertainties, we present and analyze a dataset collected in surface waters during the 19th Atlantic Meridional Transect. Results show that the relationship between particulate beam-attenuation coefficient (c_p) and chlorophyll-a concentration was consistent with published bio-optical models. In contrast, the particulate backscattering per unit of chlorophyll-a and per unit of c_p were higher than in previous studies employing the same sampling methodology. These anomalies could be due to a bias smaller than the current uncertainties in b_{bp}. If that was the case, then the AMT19 dataset would confirm that b_{bp}:c_p is remarkably constant over the surface open ocean. A second-order decoupling between b_{bp} and c_p was, however, evident in the spectral slopes of these coefficients, as well as during diel cycles. Overall, these results emphasize the current difficulties in obtaining accurate b_{bp} measurements in the oligotrophic ocean and suggest that, to first order, b_{bp} and c_p are coupled in the surface open ocean, but they are also affected by other geographical and temporal variations.

OCIS codes: 010.4450 Oceanic optics; 010.1350 Backscattering; 010.4458 Oceanic scattering.

References and links

1. IOCCG, *Remote sensing of inherent optical properties: fundamentals, tests of algorithms, and applications.*, Report Number 5 (International Ocean Colour Coordination Group, 2006).
2. J. K. B. Bishop, "Autonomous observations of the ocean biological carbon pump," Oceanography **22**, 182–193 (2009).
3. E. Boss, D. Swift, L. Taylor, P. Brickley, R. Zaneveld, S. Riser, M. J. Perry, and P. G. Strutton, "Observations of pigment and particle distributions in the western north atlantic from an autonomous float and ocean color satellite," Limnol. Oceanogr. **53**, 2112–2122 (2008).
4. N. Briggs, M. J. Perry, I. Cetinic, C. Lee, E. D'Asaro, A. M. Gray, and E. Rehm, "High-resolution observations of aggregate flux during a sub-polar north atlantic spring bloom," Deep Sea Res. Part I **58**, 1031–1039 (2011).
5. IOCCG, *Bio-optical sensors on Argo floats*, Report Number 11 (International Ocean Colour Coordination Group, 2011).
6. H. C. van de Hulst, *Light Scattering by Small Particles* (Wiley, New York, 1957).

#170689 - $15.00 USD Received 20 Jun 2012; revised 31 Aug 2012; accepted 31 Aug 2012; published 5 Sep 2012

7. H. Loisel and A. Morel, "Light scattering and chlorophyll concentration in case 1 waters: A reexamination," Limnol. Oceanogr. **43**, 847–858 (1998).
8. T. K. Westberry, G. Dall'Olmo, E. Boss, M. J. Behrenfeld, and T. Moutin, "Coherence of particulate beam attenuation and backscattering coefficients in diverse open ocean environments," Opt. Express **18**, 15419–15425 (2010).
9. A. Morel and S. Maritorena, "Bio-optical properties of oceanic waters: a reappraisal," J. Geophys. Res.-Oceans **106**, 7163–7180 (2001).
10. Y. Huot, A. Morel, M. S. Twardowski, D. Stramski, and R. A. Reynolds, "Particle optical backscattering along a chlorophyll gradient in the upper layer of the eastern south pacific ocean," Biogeosci. **5**, 495–507 (2008).
11. M. J. Behrenfeld and E. Boss, "The beam attenuation to chlorophyll ratio: an optical index of phytoplankton physiology in the surface ocean?" Deep-Sea Res. Part I**50**, 1537–1549 (2003).
12. G. Dall'Olmo, T. K. Westberry, M. J. Behrenfeld, E. Boss, and W. H. Slade, "Significant contribution of large particles to optical backscattering in the open ocean," Biogeosci. **6**, 947–967 (2009).
13. D. Antoine, D. A. Siegel, T. Kostadinov, S. Maritorena, N. B. Nelson, B. Gentili, V. Vellucci, and N. Guillocheau, "Variability in optical particle backscattering in contrasting bio-optical oceanic regimes," Limnol. Oceanogr. **56**, 955–973 (2011).
14. H. Pak, D. A. Kiefer, and J. C. Kitchen, "Meridional variations in the concentration of chlorophyll and microparticles in the north Pacific ocean," Deep Sea Res. Part A **35**, 1151–1171 (1988).
15. D. Stramski and D. Kiefer, "Light scattering by microorganisms in the open ocean," Progr. Oceanogr. **28**, 343–383 (1991).
16. A. Morel and Y. H. Ahn, "Optics of heterotrophic nanoflagellates and ciliates - a tentative assessment of their scattering role in oceanic waters compared to those of bacterial and algal cells," J. Mar. Res. **49**, 177–202 (1991).
17. Y. Ahn, A. Bricaud, and A. Morel, "Light backscattering efficiency and related properties of some phytoplankters," Deep-Sea Res. Part A **38**, 1835–1855 (1992).
18. D. Stramski, A. Bricaud, and A. Morel, "Modeling the inherent optical properties of the ocean based on the detailed composition of the planktonic community," Appl. Opt. **40**, 2929–2945 (2001).
19. M. S. Quinby-Hunt, A. J. Hunt, K. Lofftus, and D. Shapiro, "Polarized-light scattering studies of marine chlorella," Limnol. Oceanogr. **34**, 1587–1600 (1989).
20. J. C. Kitchen and J. R. V. Zaneveld, "A three-layered sphere model of the optical properties of phytoplankton," Limnol. Oceanogr. **37**, 1680–1690 (1992).
21. M. J. Behrenfeld, E. Boss, D. A. Siegel, and D. M. Shea, "Carbon-based ocean productivity and phytoplankton physiology from space," Global Biogeochem. Cy. **19**, 1–14, doi:10.1029/2004GB002299 (2005).
22. O. Ulloa, S. Sathyendranath, and T. Platt, "Effect of the particle-size distribution on the backscattering ratio in seawater," Appl. Opt. **33**, 7070–7077 (1994).
23. M. S. Twardowski, E. Boss, J. B. Macdonald, W. S. Pegau, A. H. Barnard, and J. R. V. Zaneveld, "A model for estimating bulk refractive index from the optical backscattering ratio and the implications for understanding particle composition in case I and case II waters," J. Geophys. Res.-Oceans **106**, 14129–14142 (2001).
24. A. L. Whitmire, E. Boss, T. J. Cowles, and W. S. Pegau, "Spectral variability of the particulate backscattering ratio," Opt. Express **15**, 7019–7031 (2007).
25. M. S. Twardowski, H. Claustre, S. A. Freeman, D. Stramski, and Y. Huot, "Optical backscattering properties of the "clearest" natural waters," Biogeosci. **4**, 1041–1058 (2007).
26. D. Stramski, "Relationships between the surface concentration of particulate organic carbon and optical properties in the eastern south Pacific and eastern Atlantic oceans (vol 5 pg 171, 2008)," Biogeosci. **5**, 595–595 (2008).
27. F. Nencioli, G. Chang, M. Twardowski, and T. D. Dickey, "Optical characterization of an eddy-induced diatom bloom west of the island of Hawaii," Biogeosci. **7**, 151–162 (2010).
28. A. Morel, "Optical modeling of the upper ocean in relation to its biogenous matter content (case 1 water)," J. Geophys. Res.-Oceans **93**, 10749–10768 (1988).
29. A. Morel, *Advisory Group for Aerospace Research and Development* (NATO, 1973), chap. Diffusion de la lumiere par les eaux de mer. Resultat experimentaux et approach theorique, 3.1.1–76.
30. E. Boss, M. S. Twardowski, and S. Herring, "Shape of the particulate beam attenuation spectrum and its inversion to obtain the shape of the particulate size distribution," Appl. Opt. **40**, 4885–4893 (2001).
31. E. Boss, W. H. Slade, M. Behrenfeld, and G. Dall'Olmo, "Acceptance angle effects on the beam attenuation in the ocean," Opt. Express **17**, 1535–1550 (2009).
32. H. Loisel, J. M. Nicolas, A. Sciandra, D. Stramski, and A. Poteau, "Spectral dependency of optical backscattering by marine particles from satellite remote sensing of the global ocean," J. Geophys. Res.-Oceans **111**, C09024 (2006).
33. T. S. Kostadinov, D. A. Siegel, and S. Maritorena, "Retrieval of the particle size distribution from satellite ocean color observations," J. Geophys. Res.-Oceans **114**, C09015 (2009).
34. T. S. Kostadinov, D. A. Siegel, and S. Maritorena, "Global variability of phytoplankton functional types from space: assessment via the particle size distribution," Biogeosci. **7**, 3239–3257 (2010).
35. J.M. Sullivan, C.C. Moore, M.S. Twardowski, and J.R.V. Zaneveld, "Measuring optical backscattering in water" in "*Light Scattering Reviews, Volume 7: Radiative transfer and optical properties of atmosphere and underlying*

#170689 - $15.00 USD Received 20 Jun 2012; revised 31 Aug 2012; accepted 31 Aug 2012; published 5 Sep 2012

surface" (Praxis Publishing Ltd, in press).
36. X. Zhang, L. Hu, and M.-X. He, "Scattering by pure seawater: Effect of salinity," Opt. Express **17**, 5698–5710 (2009).
37. X. Zhang and L. Hu, "Estimating scattering of pure water from density fluctuation of the refractive index," Opt. Express **17**, 1671–1678 (2009).
38. E. Boss and W. S. Pegau, "Relationship of light scattering at an angle in the backward direction to the backscattering coefficient," Appl. Opt. **40**, 5503–5507 (2001).
39. BIPM and ISO, *Guide to the Expression of Uncertainty in Measurement* (International Organization for Standardization, Geneve, Switzerland, 1995).
40. W. H. Slade, E. Boss, G. Dall'Olmo, M. R. Langner, J. Loftin, M. J. Behrenfeld, C. Roesler, and T. K. Westberry, "Underway and moored methods for improving accuracy in measurement of spectral particulate absorption and attenuation," J. Atmos. Ocean. Tech. **27**, 1733–1746 (2010).
41. J. R. V. Zaneveld, J. C. Kitchen, and C. C. Moore, "Scattering error correction of reflecting tube absorption meters," in Ocean Optics XII **2258**, S. Ackelson, ed. (SPIE, 1994), 44–55.
42. L. Van Heukelem and C. S. Thomas, "Computer-assisted high-performance liquid chromatography method development with applications to the isolation and analysis of phytoplankton pigments," J. Chromatogr. A **910**, 31–49 (2001).
43. E. S. Boss, R. Collier, G. Larson, K. Fennel, and W. S. Pegau, "Measurements of spectral optical properties and their relation to biogeochemical variables and processes in crater lake, Crater Lake National Park, OR," Hydrobiologia **574**, 149–159 (2007).
44. J. M. Sullivan and M. S. Twardowski, "Angular shape of the oceanic particulate volume scattering function in the backward direction," App. Opt. **48**, 6811–6819 (2009).
45. D. Stramski, R. A. Reynolds, M. Babin, S. Kaczmarek, M. R. Lewis, R. Rottgers, A. Sciandra, M. Stramska, M. S. Twardowski, B. A. Franz, and H. Claustre, "Relationships between the surface concentration of particulate organic carbon and optical properties in the eastern south Pacific and eastern Atlantic oceans," Biogeosci. **5**, 171–201 (2008).
46. W. M. Balch, B. C. Bowler, D. T. Drapeau, A. J. Poulton, and P. M. Holligan, "Biominerals and the vertical flux of particulate organic carbon from the surface ocean," Geophys. Res. Lett. **37**, L22605– (2010).
47. R. J. Geider, "Light and temperature dependence of the carbon to chlorophyll a ratio in microalgae and cyanobacteria: implications for physiology and growth of phytoplankton," New Phytol. **106**, 1–34 (1987).
48. A. Morel, "Chlorophyll-specific scattering coefficient of phytoplankton a simplified theoretical approach," Deep-Sea Res. Part I **34**, 1093–1106 (1987).
49. H. L. MacIntyre, T. M. Kana, T. Anning, and R. J. Geider, "Photoacclimation of photosynthesis irradiance response curves and photosynthetic pigments in microalgae and cyanobacteria," J. Phycol. **38**, 17–38 (2002).
50. H. R. Gordon and A. Morel, *Remote Assessment of Ocean Color for Interpretation of Satellite Visible Imagery. A Review* (Springer-Verlag, New York, 1983).
51. D. A. Hansell, C. A. Carlson, D. J. Repeta, and R. Schlitzer, "Dissolved organic matter in the ocean: A controversy stimulates new insights," Oceanography **22**, 202–211 (2009).
52. I. Koike, S. Hara, K. Terauchi, and K. Kogure, "Role of sub-micrometre particles in the ocean," Nature **345**, 242–244 (1990).
53. P. H. Santschi, E. Balnois, K. J. Wilkinson, J. W. Zhang, J. Buffle, and L. D. Guo, "Fibrillar polysaccharides in marine macromolecular organic matter as imaged by atomic force microscopy and transmission electron microscopy," Limnol. Oceanogr. **43**, 896–908 (1998).
54. Y. P. Shao, K. H. Wyrwoll, A. Chappell, J. P. Huang, Z. H. Lin, G. H. McTainsh, M. Mikami, T. Y. Tanaka, X. L. Wang, and S. Yoon, "Dust cycle: An emerging core theme in earth system science," Aeolian Res. **2**, 181–204 (2011).
55. M. Jonasz and G. Fournier, "Approximation of the size distribution of marine particles by a sum of log-normal functions," Limnol. Oceanogr. **41**, 744–754 (1996).
56. R. Astoreca, D. Doxaran, K. Ruddick, V. Rousseau, and C. Lancelot, "Influence of suspended particle concentration, composition and size on the variability of inherent optical properties of the southern North Sea," Cont. Shelf Res. **35**, 117–128 (2012).
57. K. Oubelkheir and A. Sciandra, "Diel variations in particle stocks in the oligotrophic waters of the Ionian Sea (Mediterranean)," J. Mar. Syst. **74**, 364–371 (2008).
58. G. Dall'Olmo, E. Boss, M. J. Behrenfeld, T. K. Westberry, C. Courties, L. Prieur, M. Pujo-Pay, N. Hardman-Mountford, and T. Moutin, "Inferring phytoplankton carbon and eco-physiological rates from diel cycles of spectral particulate beam-attenuation coefficient," Biogeosci. **8**, 3423–3439 (2011).
59. M. D. DuRand and R. J. Olson, "Contributions of phytoplankton light scattering and cell concentration changes to diel variations in beam attenuation in the equatorial pacific from flow cytometric measurements of pico-, ultra- and nanoplankton," Deep-Sea Res. Part II **43**, 891–906 (1996).
60. H. Claustre, A. Morel, M. Babin, C. Cailliau, D. Marie, J. C. Marty, D. Tailliez, and D. Vaulot, "Variability in particle attenuation and chlorophyll fluorescence in the tropical Pacific: Scales, patterns, and biogeochemical implications," J. Geophys. Res.-Oceans **104**, 3401–3422 (1999).

#170689 - $15.00 USD Received 20 Jun 2012; revised 31 Aug 2012; accepted 31 Aug 2012; published 5 Sep 2012

61. R. A. Maffione, and D. R. Dana, "Instruments and methods for measuring the backward-scattering coefficient of ocean waters," Appl. Opt. **36**, 6057–6067 (1997).

1. Introduction

Ocean biogeochemical cycles are tightly linked to the dynamics of suspended particles such as phytoplankton, heterotrophic organisms, detritus, and minerals. Understanding these dynamics is an important objective of oceanographic research and much can be learned by interpreting optical scattering measurements. Optical scattering can be measured remotely either by inversion of satellite ocean color data [1] or by in situ autonomous platforms, such as floats and gliders [2–5]. Unraveling the links between optical scattering and the concentrations and characteristics of oceanic particles, therefore, has the potential of extending the range over which these particles and their dynamics can be observed.

The following inherent optical properties are typically employed to characterize the scattering of light by marine particles: the particulate backscattering, scattering, and beam-attenuation coefficients (b_{bp}, b_p, and c_p, respectively). Note that b_p and c_p are approximately equal in clear waters, due to the low influence of particulate absorption (a_p) on c_p [7, 8].

Previous studies demonstrated that b_{bp}, b_p and c_p are to first order correlated to the concentration of chlorophyll-a (*Chl*), which is often considered an index of phytoplankton abundance [7,9,10]. More recently, however, it has been shown that these relationships are inherently noisy, because the *Chl* signal is strongly impacted by physiological variability [8, 11–13].

The particulate optical scattering is thought to be generated by particles in the phytoplankton size range (0.5-20 μm, e.g., ref. [14, 15]). The particle size domain responsible for b_{bp}, on the other hand, remains uncertain. Some studies suggest that b_{bp} is governed by submicron detrital particles and minerals [15–18], while others have shown the importance of larger particles (including phytoplankton cells) in generating the observed b_{bp} variability [12, 19, 20].

The particulate backscattering efficiency (b_{bp}:b_p) is less dependent on the absolute concentration of particles than either property alone and is largely governed by particle size, composition, and morphology [22, 23]. Highly refractive particles, such as the minerals contained in atmospheric dust or coccolithophorids, are expected to be associated with high b_{bp}:b_p [22–24]. On the other hand, b_{bp}:b_p for a given particle composition should, to first order, increase when small particles become relatively more abundant than large particles [22, 23]. However, the uncertainties on the sources of b_p and b_{bp} as well as potential limitations in current optical models of oceanic particles may limit the interpretation of the b_{bp}:b_p ratio.

Experimental studies have demonstrated a relatively large range of variation for b_{bp}:b_p (i.e., approximately 0.2%-2%, refs. [8, 12, 13, 24–26]), in part due to difficulties in accurately determining b_{bp} in clear oligotrophic waters. Nevertheless, a surprisingly coherent value for b_{bp}:b_p of around 1% was recently reported in diverse surface open-ocean waters, using data from a series of cruises where scattering measurements were conducted using a consistent methodology [8]. Although other studies have also measured similar backscattering ratios [24], this finding suggests that methodology may be an important source of uncertainty in b_{bp} and b_p measurements, especially in clear oligotrophic waters.

Both c_p and b_{bp} vary spectrally and their spectral dependency is commonly modelled as a power law [28]:

$$c_p(\lambda) = c_p(\lambda_0)\left(\frac{\lambda}{\lambda_0}\right)^{-\gamma_{cp}} \tag{1}$$

$$b_{bp}(\lambda) = b_{bp}(\lambda_0)\left(\frac{\lambda}{\lambda_0}\right)^{-\gamma_{bbp}} \tag{2}$$

#170689 - $15.00 USD Received 20 Jun 2012; revised 31 Aug 2012; accepted 31 Aug 2012; published 5 Sep 2012

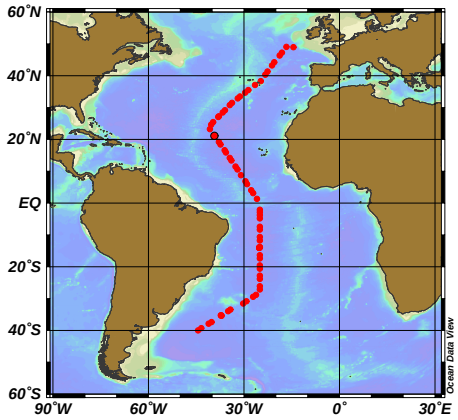

Fig. 1. Locations of CTD casts during AMT19 indicating the cruise track. Background colors represent the bathimetry.

where γ_{cp} and γ_{bbp} are the spectral slopes of c_p and b_{bp}, respectively, and λ_0 is a reference wavelength. If particles are non-absorbing and their sizes are distributed according to a power law with exponent η over the entire range of particle sizes, then $\gamma_{cp} \cong \eta - 3$ (Voltz, 1954 cited in ref. [6]; [29]; see also [30]). This latter equation establishes a link between the spectral properties of c_p and the relative distribution of large vs. small particles and it has been verified with in situ measurements from coastal waters [30]. A drawback of using the spectral slope of c_p to infer information on the particle size distribution is that the particulate beam-attenuation coefficient cannot be determined from space. Moreover, due to the finite acceptance angle of commercial instruments, c_p and b_p are never exactly measured [31].

Loisel et al. (2006) inverted space-based ocean color measurements to estimate the spectral slope of b_{bp} [32]. These authors found that γ_{bbp} exhibited positive values (relatively more small particles) in oligotrophic waters and negative values (relatively more large particles) in more eutrophic waters. Building on this insight, Kostadinov and collaborators [33] developed an inversion algorithm to relate γ_{bbp} to the slope of the particle size distribution and produced global maps of the abundances of three different size classes of phytoplankton [34].

Despite these developments, simultaneous measurements of b_p and b_{bp} in the open ocean are still limited, especially in oligotrophic regions. Here, we present and analyze a dataset of particulate scattering and backscattering measurements collected during the 19th Atlantic Meridional Transect (AMT19). Our main objectives are to investigate the variability of b_{bp} and c_p and to test existing bio-optical relationships. We show that b_{bp} was relatively high in the Atlantic compared to previous data from other oceanic regions. This discrepancy could either be due to a more significant contribution from particles smaller than 0.2 μm or, most likely, to a small bias in our measurements. In the latter case, this analysis confirms that the shape of the volume scattering function of marine particles is remarkably constant.

2. Methods

Data were collected on board the *RRS James Cook* from October 13th to December 1st 2009 covering a meridional transect approximately from 45°N to 40°S (Fig. 1).

#170689 - $15.00 USD Received 20 Jun 2012; revised 31 Aug 2012; accepted 31 Aug 2012; published 5 Sep 2012

Table 1. Scaling factors for the BB349 and BB499 meters. "Final values" are those used to process the data presented in this study. Absolute uncertainties are standard error of the means of the AMT19 determinations. All values, except relative uncertainties, are in units of sr^{-1} $counts^{-1} \times 10^{-6}$. Number in parentheses are percent changes from the WetLabs (07/2009) calibration.

	BB349			BB499		
	470	526	656	470	526	595
WetLabs (07/2009)	6.641	4.349	2.168	6.947	4.396	2.660
AMT19 (20/10/2009)	6.432(−3.2)	4.496(+3.4)	2.323 (+7.1)	7.347(+5.8)	4.975(+13.2)	-
AMT19 (22/11/2009)	6.771 (+2.0)	4.539(+4.4)	2.624(+21.0)	7.216(+3.9)	4.590 (+4.4)	2.535(-4.7)
Final values	6.601	4.517	2.473	7.281	4.782	2.598
Abs. uncertainties	0.170	0.021	0.151	0.066	0.192	0.063
Rel. uncertainties	0.026	0.005	0.061	0.009	0.040	0.024

Table 2. Dark counts provided by manufacturer and measured during AMT19. Uncertainties represent half the central 68th percentile of the measurements conducted during AMT19. All units are counts.

	BB349			BB499		
	470	526	656	470	526	595
WetLabs	52	46	42	44	42	27
AMT19	56	51	50	53	48	50
AMT19 uncertainties	1.0	1.5	1.5	2.0	2.0	1.5

2.1. Flow through optical measurements

Optical measurements were conducted on seawater from the ship's clean flow-through system pumped from a depth of about 5 m. The methodology described in ref. [12] was followed, including one-minute data binning and the use of a 0.2μm-cartridge filter (Cole Parmer) through which the water supply was diverted every hour for ten minutes to provide a baseline for particulate absorption and attenuation measurements.

2.1.1. b_{bp}

Continuous b_{bp} measurements were made using a WET Labs ECO-BB3 meter (S/N 349, thereafter referred to as BB349) in a flow-through chamber, as described in ref. [12]. The characterization of the instrument included an evaluation of the effective wavelengths as described in ref. [12]. The instrument was calibrated by the manufacturer in July 2009. In addition, we conducted calibrations at the beginning (Oct. 20th, 2009) and end (Nov. 22nd, 2009) of the cruise, following the same protocol adopted for our previous studies [8, 12] and described in the Appendix. Table 1 reports the results of these calibrations and shows that the blue and green channels were relatively stable, while the scaling factor of the red channel (656 nm) varied by 21% from the factory calibration. Because of this drift, data from the red channel were not used in this analysis.

Three dark counts determinations were carried out during the cruise (yeardays 293, 313, and 326) by covering the detectors with black tape and submerging the instrument in water. Results from these independent replicate measurements indicated that the dark counts varied at most by 2 counts in the blue and green channels, but as much as 6 counts in the red channel (Table 2). In addition, the dark counts determined during the cruise differed considerably from those provided by the manufacturer.

Average scaling factors, S, and dark counts, D, measured during the cruise were employed in the processing of the BB349 data. The contribution to b_{bp} by reflections from the internal walls of the flow-through chamber, $b_{b,\mathrm{wall}}$, was determined in the laboratory (following the

#170689 - $15.00 USD Received 20 Jun 2012; revised 31 Aug 2012; accepted 31 Aug 2012; published 5 Sep 2012

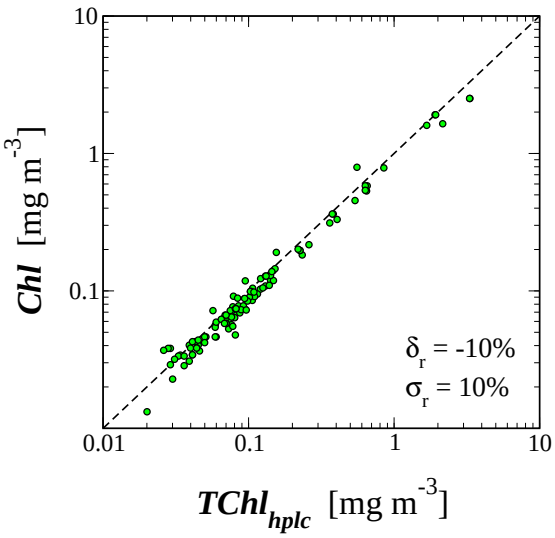

Fig. 2. Comparison between *Chl* estimated from the AC9 and ACs instruments and HPLC derived TChl. The dashed line is the 1:1 line. $N = 109$. δ_r and σ_r are robust estimates of relative bias (median of the relative residuals) and precision (σ_{68} of the relative residuals), respectively.

procedure described in ref. [12]) after the cruise and found to be $(3.70 \pm 0.83) \times 10^{-4}$ m^{-1} and $(3.14 \pm 0.52) \times 10^{-4}$ m^{-1} for the blue and green channels, respectively. Calculation of the particulate backscattering coefficient was conducted as in ref. [12], after subtracting the contribution of pure sea water, β_{sw} (differences in temperature and salinity were accounted for using data from the ship's underway CTD system; [36,37]) and using a χ_p factor of 1.1 to relate the volume scattering function at 117° to b_{bp} [38]:

$$b_{bp} = 2\pi\chi_p[S(C-D) - \beta_{sw}] - b_{b,\text{wall}} \tag{3}$$

where C are the digital counts recorded by the instrument. Finally, the particulate b_{bp} of water that passed through a 0.2 μm filter (hereafter b_{b02}) was estimated from the BB349 measurements conducted each hour on the 0.2μm-filtered seawater (details of these calculations can be found in reference [12]).

To understand how the uncertainty in dark counts affects the resulting b_{bp} values, the entire BB349 dataset was reprocessed using the dark counts supplied by the manufacturer. Resulting b_{bp} values were then compared to those derived using dark counts measured during the cruise. Relative differences ranged from 5% to 25% (not shown), with largest values in the clearest waters. This analysis demonstrates the importance of employing field-based determinations of dark counts for achieving maximally accurate b_{bp} estimates in oligotrophic regions [25].

The combined uncertainty in b_{bp} due to the uncertainties in all its input parameters (Tables 3, 4) was computed using the standard law of propagation of uncertainty [39] and assuming uncorrelated uncertainties. The median absolute uncertainties were 3.3×10^{-4} m^{-1} and 2.5×10^{-4} m^{-1}, for the blue and green channels, respectively. Relative uncertainties in b_{bp} ranged approximately from 20% in eutrophic waters to 40% in oligotrophic waters.

Given that b_{bp} was accurately determined only at two wavelengths, γ_{bbp} was derived as $\gamma_{bbp} = -\log[b_{bp}(470)/b_{bp}(526)]/\log(470/526)$. These γ_{bbp} values should be treated with caution, as they may be affected by uncertainties due to the limited number of wavelengths employed in the computation.

#170689 - $15.00 USD Received 20 Jun 2012; revised 31 Aug 2012; accepted 31 Aug 2012; published 5 Sep 2012

Table 3. Uncertainties used to compute the combined experimental uncertainty of b_{bp} as a function of wavelength. Units of absolute uncertainties are the same as those reported in the text for the corresponding variables.

Variable	BB349		BB499		Reference
	470 nm	526 nm	470 nm	526 nm	
χ_p	2.9%	2.9%	2.9%	2.9%	[44]
S	10%	10%	10%	10%	[35]
C	1.5	2.5	3.0	2.5	measured
D	1.0	1.5	2.0	2.0	measured
β_{sw}	2.24%	2.24%	2.24%	2.24%	[36]
$b_{b,\text{wall}}$	8.3×10^{-5}	5.2×10^{-5}	-	-	measured

2.1.2. c_p, a_p, and b_p

Spectrally-resolved particulate beam-attenuation, c_p, and absorption, a_p, measurements were conducted with WET Labs ACs (hyperspectral between 400 and 750 nm, with a spectral resolution of 5 nm and a band pass of 15 nm) and AC9 (nine wavelengths between 412 and 715 nm, with a band pass of 10 nm) absorption and attenuation meters. The ACs was used from the beginning of the cruise, but after 13 days (i.e., yearday 299) the lamp of the attenuation channel (i.e., C-channel) failed. To ensure continuous measurements of spectral c_p after the ACs failure, the AC9 meter was added to the flow-through system, without removing the ACs. c_p and a_p for the ACs were computed after subtraction of baseline signals derived from the 0.2μm-filtered water following established protocols [12, 40]. a_p for the AC9 meter was computed by subtracting the 0.2μm-filtered signal and applying a scattering correction [41]. Particulate scattering coefficients, b_p, were derived as the difference between c_p and a_p. AC9 measurements were linearly interpolated to derive c_p and b_p at 470 and 526 nm. The spectral slope of c_p, γ_{cp}, was estimated by fitting Eq. (1) to c_p spectra.

2.1.3. *Chl*

Discrete water samples (2-4 liters) were collected from the flow-through system during the cruise, filtered onto Whatman GF/F filters and immediately stored in liquid nitrogen. Phytoplankton pigments were determined in the laboratory after the cruise by high performance liquid chromatography (HPLC) analysis [42]. Total chlorophyll-a concentration (TChl-a) was calculated by summing the contributions of monovinylchl-a, divinyl-chl-a (DivChl-a), and chlorophyllide a.

The concentration of chlorophyll-a (*Chl*) was also estimated from the a_p line height around 676 nm as: $Chl = [a_p(676) - 39/65a_p(650) - 26/65a_p(715)]/0.014$, ref. [43]. While the AC9 instrument outputs measurements at 650, 676, and 715 nm, the ACs does not. Therefore, the ACs data were linearly interpolated to estimate a_p values at 650, 676, and 714 nm.

As mentioned above, two different instruments (i.e., ACs and AC9) were employed to measure a_p and estimate *Chl* during the cruise. Therefore, an intercalibration was required to make *Chl* estimated from the ACs a_p data comparable to the *Chl* derived from the AC9 a_p data. Simultaneous measurements of a_p by the ACs and AC9 instruments were, however, available only after the failure of the ACs C-channel, used for the scattering correction required to derive the a_p data. Thus, although simultaneous measurements of a_p from the two instruments were available, the a_p spectra derived from the ACs instrument could not be scattering corrected and thus were, in principle, not comparable to the AC9 a_p spectra. The sensitivity of the a_p-based *Chl* on the scattering correction was therefore investigated by exploiting the ACs a_p measurements collected at the beginning of the cruise, when the ACs C-channel was still functioning. The first

#170689 - $15.00 USD Received 20 Jun 2012; revised 31 Aug 2012; accepted 31 Aug 2012; published 5 Sep 2012

Table 4. Uncertainty budget for b_{bp} based on the values presented in Table 3 and on all backscattering measurements collected during the cruise in flow-through mode (BB349). Numbers represent the median values of the squared percent contributions, σ^2_{rel} (unitless), and the median absolute contributions, σ (m^{-1}), by each input variable to the combined experimental uncertainty in b_{bp} as a function of wavelength.

Variable	σ^2_{rel}		$\sigma \times 10^{-4}$	
	470 nm	526 nm	470 nm	526 nm
χ_p	1	1	0.28	0.24
S	85	81	3.01	2.19
C	5	9	0.68	0.78
D	2	4	0.46	0.47
β_{sw}	1	1	0.38	0.23
$b_{b,\text{wall}}$	6	4	0.83	0.52

13 days of ACs a_p data were reprocessed without applying any scattering and residual temperature corrections and *Chl* was derived from these newly processed a_p spectra. The ratio between *Chl* derived from the ACs with and without the scattering correction was statistically indistinguishable from one (median $\pm$ σ_{68} = 1.03 ± 0.08, where σ_{68} is half the central 68$^{\text{th}}$ percentile range and is equivalent to one standard deviation, if the data are normally distributed). This result indicates that *Chl* can be computed from the ACs a_p spectra, even if a scattering correction is not implemented. We therefore compared the *Chl* values estimated from the simultaneous AC9 and ACs a_p data collected after the failure of the ACs C-lamp, even though no scattering correction could be applied to the ACs a_p data. The ratio of these ACs-to-AC9 *Chl* was found to be 0.69 ± 0.08 (median $\pm$ σ_{68}), indicating that the *Chl* derived from the ACs was about 30% lower than that derived from the AC9. This difference is likely due to the "band pass" of the AC9 that is narrower (10 nm) than that of the ACs (15 nm). The median ACs-to-AC9 *Chl* ratio was finally employed to correct the *Chl* derived from the AC9 data.

Figure 2 compares coincident HPLC-derived TChl-a and optically-determined *Chl* (derived from both AC9 and ACs instruments) and shows that the optically-determined *Chl* was underestimated by about 10% (in median) and had a precision (σ_{68} of relative residuals) of about 10%. The 10% bias was removed from *Chl* for the rest of the analysis.

2.2. Measurements of b_{bp} from profiling package

An independent WetLabs ECO-BB3 backscattering meter (S/N 499, hereafter BB499) was installed on a profiling package that was deployed daily. The instrument was equipped with spectral channels at 470, 526, and 595 nm.

A calibration based on beads was not completed for this instrument at the beginning of the cruise. However, an intercalibration between flow-through and profiling meters was conducted at the beginning of the cruise (Oct. 16$^{\text{th}}$-18$^{\text{th}}$, 2009). This inter comparison consisted of collecting coincident data with the two meters by temporarily installing the profiling meter in a flow-through chamber similar to that where the flow-through meter was installed. Scaling factors, S^i_{499}, for the profiling BB499 meter were derived as $S^i_{499} = \langle S_{349}(C^i_{499} - D_{499})/(C^i_{349} - D_{349})\rangle$, where each variable depends on wavelength, S_{349} is the scaling factor derived for the flow-through instrument as the average of the two cruise calibrations, C^i_{349} and C^i_{499} are the coincident raw counts recorded by the two instruments, D_{349} and D_{499} are the corresponding dark counts, and the $\langle\rangle$ brackets indicate that the median value was taken. In addition, a standard calibration was completed towards the end of the cruise using a dilution series of NIST-traceable 2-μm polystyrene beads, Thermo Scientific). The relative differences between the scaling factors de-

#170689 - $15.00 USD Received 20 Jun 2012; revised 31 Aug 2012; accepted 31 Aug 2012; published 5 Sep 2012

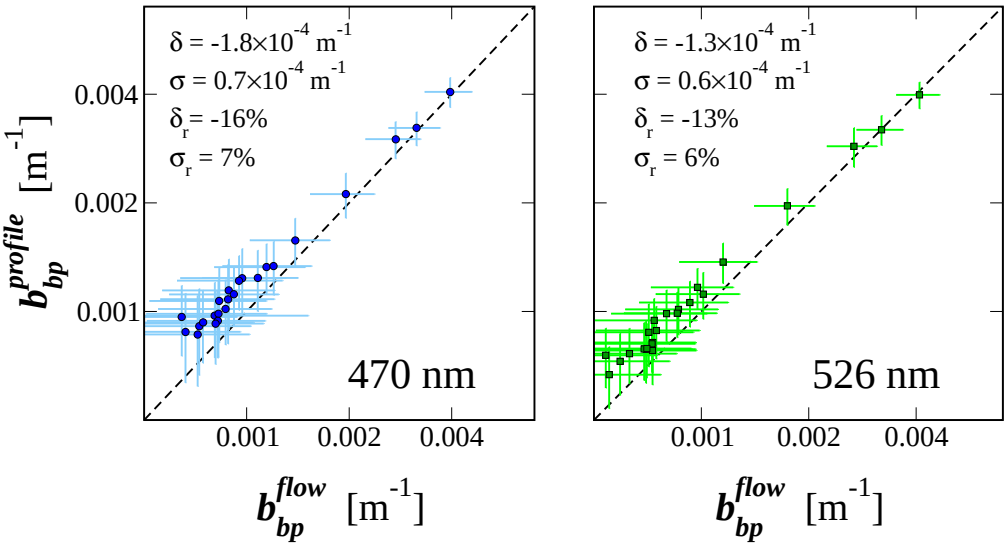

Fig. 3. Comparison between b_{bp} measurements collected at two different wavelengths by the instruments mounted on the flow-through and profiling systems. Error bars represent the combined uncertainties in the b_{bp} estimates. Dashed lines are the 1:1 lines. Note the logarithmic scales on all axes. δ and δ_r are robust estimates of the absolute and relative bias, respectively. σ and σ_r are estimates (σ_{68} of residuals) of the absolute and relative precision, respectively. $N = 24$.

rived from the intercalibration and standard calibration and those provided by the factory are presented in Table 1. Dark counts were also measured during the cruise and showed significant deviations from those provided by the manufacturer (Table 2). However, these D_{499} value were not determined with the BB499 instrument installed on the profiling package and thus could be biased. Data from the 595-nm channel were excluded from the rest of the analysis because of the unexplained large change (23 counts) in its dark counts. The b_{bp} values and corresponding uncertainties derived from the profiling instrument (BB499) were computed following the same methodology employed for the flow-through instrument (BB349) (for in-water measurements no correction for wall effects was needed).

Median b_{bp} data were extracted from each upcast profile between 4 and 10 meters to match the depth of the ship's water intake. A comparison of coincident b_{bp} values determined by the two independently-calibrated and deployed instruments indicated biases of -16% and -13% and precisions of 7% and 6% for the 470 and 526 nm channels, respectively (Fig. 3). The above biases may be due to uncertainties in dark counts, that were determined with the instrument connected to an electrical system (i.e., power supply and cables) different from the one used to collect measurements.

3. Results

Chl, b_{bp} and b_p displayed largest values in temperate and tropical regions and minimal values in the subtropical gyres (Fig. 4). *Chl* varied by over two orders of magnitude, while b_{bp} and b_p varied by over one order of magnitude. The broadscale patterns of $b_{bp}(526)$ and *Chl* were in agreement with previous measurements in the Atlantic ocean [45, 46]. The particulate backscattering vs. *Chl* relationship obtained during AMT19 was also in general agreement existing bio-optical models, although $b_{bp}(526)$ was underestimated by existing models at low *Chl*

#170689 - $15.00 USD Received 20 Jun 2012; revised 31 Aug 2012; accepted 31 Aug 2012; published 5 Sep 2012

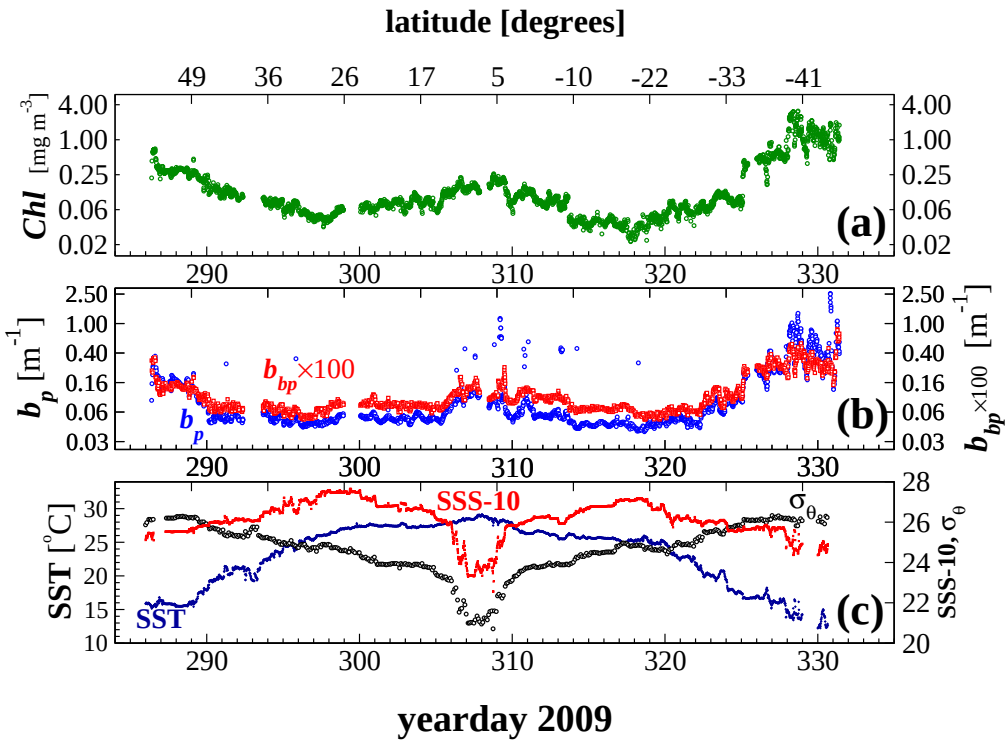

Fig. 4. Time series of *Chl*, $b_{bp}(526)$ and $b_p(526)$, sea surface temperature (SST), salinity (from which a constant value of 10 psu was subtracted for plotting purposes, SSS-10, psu) and potential density anomaly (σ_θ, kg m^{-3}).

(Fig. 5(a)). On the other hand, $b_p(526)$ agreed better with existing bio-optical models (Fig. 5(b), [10, 12]).

The particulate backscattering ratio, b_{bp}:b_p, varied latitudinally, with maximum values ($\sim$ 0.02) in oligotrophic regions and minimum values in the eutrophic waters (< 0.01, Fig. 6(a)). An important fraction of this variability ($\sim$ 30%) appeared to be due to variations occurring at the diel scale. The chlorophyll-specific particulate scattering and backscattering coefficients (b_p^* and b_{bp}^*, respectively) varied by over an order of magnitude along the transect with maximum values in the most oligotrophic regions and also showed strong diel cycles (Fig. 6(b)). Finally, the spectral slopes of b_{bp} and c_p (γ_{bbp} and γ_{cp}, respectively) were inversely correlated, with γ_{cp} displaying higher values in productive regions and lower values in the most oligotrophic waters (Fig. 6(c)). Strong variations of γ_{cp} were observed at the end of the transect in the most productive region sampled. While γ_{cp} appeared to be affected by diel cycles, γ_{bbp} did not.

Particulate absorption contributed, as expected, only a relatively small fraction of c_p (data not shown): the largest values of a_p:c_p were found at 440 nm ($8-16$%, 95$^{\text{th}}$ percentile range), while minimum values were found for wavelengths smaller than 532 nm ($2-6$%). The ratio of particulate backscattering to beam-attenuation at 526 nm, b_{bp}:c_p, ranged from less than 0.002 to 0.020, with a median value ($\pm$ σ_{68}) of 0.0130 ± 0.0032 (Fig. 7, solid line). b_{bp}:c_p values measured during AMT19 were skewed towards higher values than those of previously published datasets [8].

The backscattering signal measured on 0.2μm filtered samples after subtraction of the pure seawater signal (i.e., b_{b02}) varied latitudinally with larger values in the most productive regions

#170689 - $15.00 USD Received 20 Jun 2012; revised 31 Aug 2012; accepted 31 Aug 2012; published 5 Sep 2012

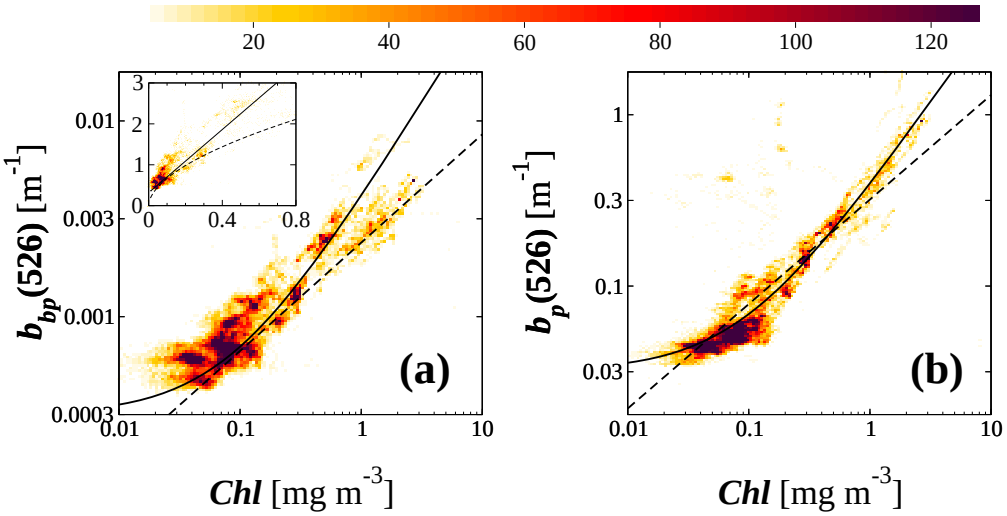

Fig. 5. Bivariate histograms showing the relationships between $b_{bp}(526)$ and $b_p(526)$ versus *Chl*. Solid and dashed lines are the models presented in refs. [12] and [10], respectively. The inset presents the $b_{bp}(526)$ vs. *Chl* bivariate histogram, but in linear scale (b_{bp} is multiplied by 1000). The colorbar identifies the number of data points in each bivariate bin.

of the transect (Fig. 8). 95% confidence intervals suggest that b_{b02} was not significantly higher than zero along most of the transect (Fig. 8). This finding is in agreement with a previous study that reported negligible b_{b02} values in the surface equatorial Pacific [12], although the average b_{b02} values measured during AMT19 appeared larger than previously observed. b_{b02} contributed a relatively important fraction of b_{bp}: 0.19 ± 0.06 and 0.11 ± 0.04 at 470 and 526 nm, respectively (Fig. 8). b_{b02} was positively, but weakly related to *Chl* and bulk values of c_p, b_{bp} and a_p (not shown).

4. Discussion

4.1. b_{bp}:Chl, b_p:Chl

In this study, a dataset of surface optical scattering measurements collected along the 19th Atlantic Meridional Transect is presented. As previously observed, b_{bp} and b_p were, to first order, related to *Chl* [8, 10, 12, 13], although considerable variability exists in these relationships. At least three reasons may explain this relatively large variability. First, changes in the ratio of backscattering to *Chl* may register changes in the phytoplankton carbon-to-*Chl* ratio associated with changes in phytoplankton acclimation to the diverse temperature, nutrient, light environments, and species compositions encountered during the transect [8, 11, 21, 47–49]. Second, since the AMT samples a wide range of ecological provinces, the large variability observed in b_{bp}:*Chl* may have also been driven by changes in the efficiency with which phytoplankton backscatter light due to variations in cell size, composition, and morphology. Third, b_{bp}:*Chl* may depend on both phytoplankton (driving changes in *Chl*) and other particles (mostly driving changes in b_{bp}) and the coupling between these drivers may vary with the trophic status of the ocean [13, 48, 50]. Most likely, a combination of these factors explains the observed variability in the b_p^* and b_{bp}^* ratios.

#170689 - $15.00 USD Received 20 Jun 2012; revised 31 Aug 2012; accepted 31 Aug 2012; published 5 Sep 2012

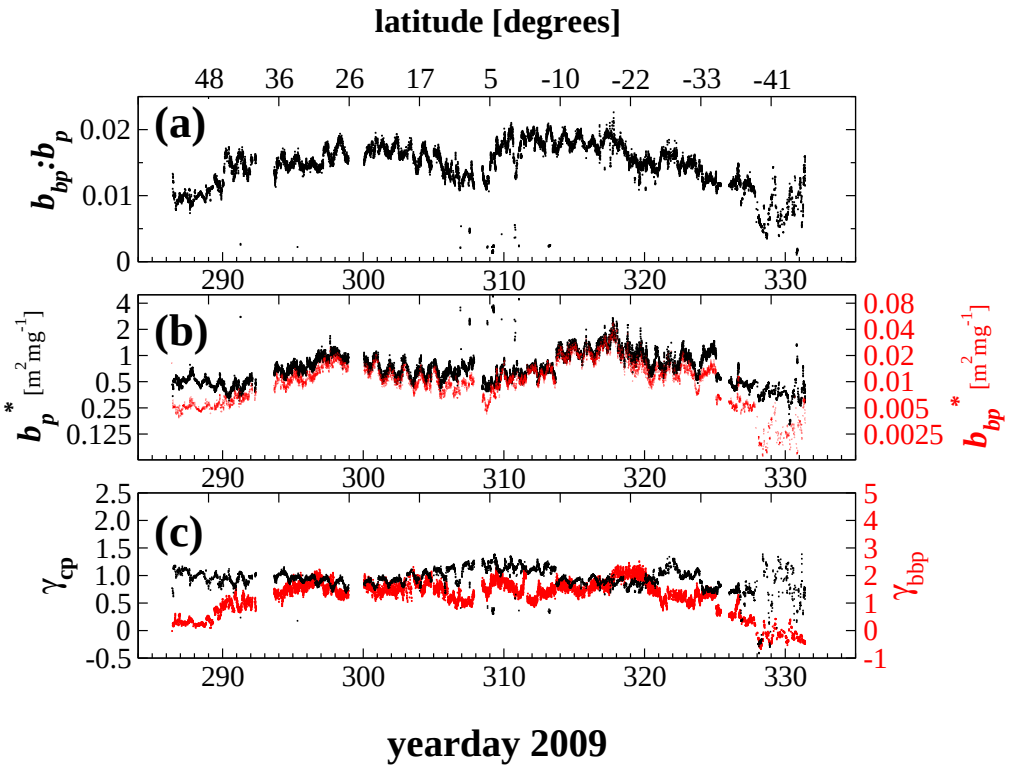

Fig. 6. Time series of b_{bp}:b_p at 526 nm, chl-specific b_p(526) and b_{bp}(526) (b_p^* and b_{bp}^*, respectively; m^2 mg^{-1}) and the spectral slopes of c_p (γ_{cp}) and b_{bp} (γ_{bbp}).

4.2. b_{bp}:c_p

The b_{bp}:c_p ratio over most of the transect was higher than in previous cruises that employed the same flow-through methodology [8,12]. This observation, if verified, is at odds with the findings of refs. [12] and [8] that there is a consistent relationship between b_{bp} and c_p in the surface open ocean. These authors argued that, since the particulate beam-attenuation coefficient is likely controlled by variations in phytoplankton carbon biomass, then a consistent b_{bp}:c_p ratio would imply that one could estimate c_p, and thus phytoplankton carbon, from remotely sensed b_{bp} [8, 12, 21]. Results from the analysis of the AMT19 dataset suggest that such endeavour might be more complex than previously thought and could require regional parametrizations. Alternatively, the deviation of the measured b_{bp}:c_p ratio from published values could be also due to a small bias in b_{bp} ($\sim 1 \times 10^{-4}$ m^{-1} at 526 nm; see sections 4.3 and 4.4). Importantly, this bias is smaller than the median uncertainty of our b_{bp} measurements ($\sim 2.5 \times 10^{-4}$ m^{-1} at 526 nm, Table 4).

Previous studies reported b_{bp}:b_p measurements from two independent datasets of optical scattering collected in the ultra-oligotrophic South Pacific sub-tropical gyre [25,26,45]. Despite the general agreement demonstrated between the b_{bp} values measured in these two datasets [25], the near-surface b_{bp}:b_p values reported showed considerable variability ranging from less that 0.004 at 650 nm (Fig. 5 in ref. [25]) to more than 0.015 at 555 nm (Fig. 11 in [26]). These large discrepancies are unexpected given the relatively neutral spectral shape of b_{bp}:b_p (refs. [22, 24, 25]). However, although in the more productive waters the b_{bp}:b_p ratio at 555 nm was relatively stable and similar to the average value reported in ref. [8], higher values of

#170689 - $15.00 USD Received 20 Jun 2012; revised 31 Aug 2012; accepted 31 Aug 2012; published 5 Sep 2012

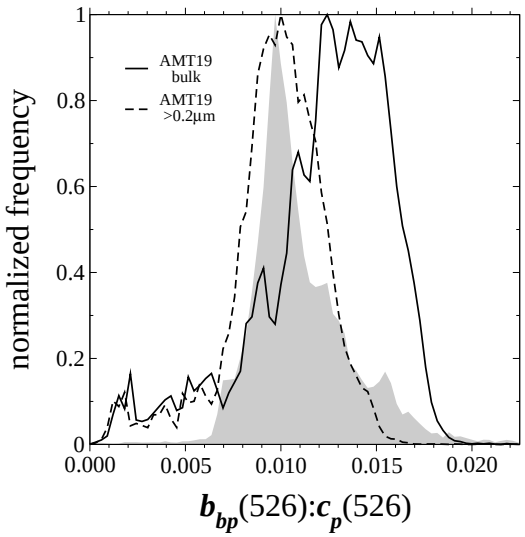

Fig. 7. Normalized frequency distribution of b_{bp}:c_p measured during AMT19 (solid line) and of $(b_{bp}-b_{b02})$:c_p (dashed line). All measurements are at 526 nm. The shaded area represents the mean value of the normalized frequency distributions of the datasets presented in ref. [8].

b_{bp}:b_p were observed in the most oligotrophic waters sampled ($Chl < 0.075-0.100$ mg m^{-3} see Figs. 2 and 11 in [26, 45]). The b_{bp}:b_p values recorded during AMT19 were also maximal in the most oligotrophic waters (Figs. 4 and 6). This similarity suggests that the increase of b_{bp}:b_p in oligotrophic waters could be a general bio-optical feature [9, 28] or could be related to a decrease in the achievable b_{bp} accuracy in very clear waters.

4.3. b_{b02}

The backscattering measured on sample water that passed through the 0.2-μm filter was found to be higher than zero, although not significantly at the 95% confidence level, and contributed about 10% of the b_{bp} signal at 526 nm (Fig. 8). Previously, $b_{b02}(526)$ was found to be indistinguishable from zero (at the 95% confidence level) in the Equatorial Pacific [12] and in the Mediterranean Sea (Dall'Olmo G., unpublished data), or significantly higher than zero, but negligible with respect to the bulk b_{bp}, in the North Atlantic and North Pacific (Westberry T.K., unpublished data).

It is important to recognize that b_{b02} may not accurately represent the backscattering of colloids smaller than 0.2 μm. This is because it may be affected by biases due to the use of filters to partition the particle size distribution, including particle breakage and retention of particles smaller than the nominal pore size (see discussion in ref. [12]). However, the same methodology was employed in the current and previous studies. Thus, similar biases should apply, which supports the comparison of b_{b02} values between cruises. Excessive clogging of filters or particle accumulation on the optical surface of the flow-through instrument were limited during AMT19, as shown by the negligible changes in b_{b02} after filters were replaced and after the flow-through system was cleaned, respectively (Fig. 8). Therefore, the unusually high b_{b02} values measured during AMT19 could either represent the contribution of particles smaller than 0.2 μm to the bulk b_{bp} coefficient, or reflect the magnitude of the small bias that seems to affect our b_{bp} measurements.

To quantify the importance of b_{b02} on the observed b_{bp}:c_p ratio, we subtracted b_{b02} from b_{bp}

#170689 - $15.00 USD Received 20 Jun 2012; revised 31 Aug 2012; accepted 31 Aug 2012; published 5 Sep 2012

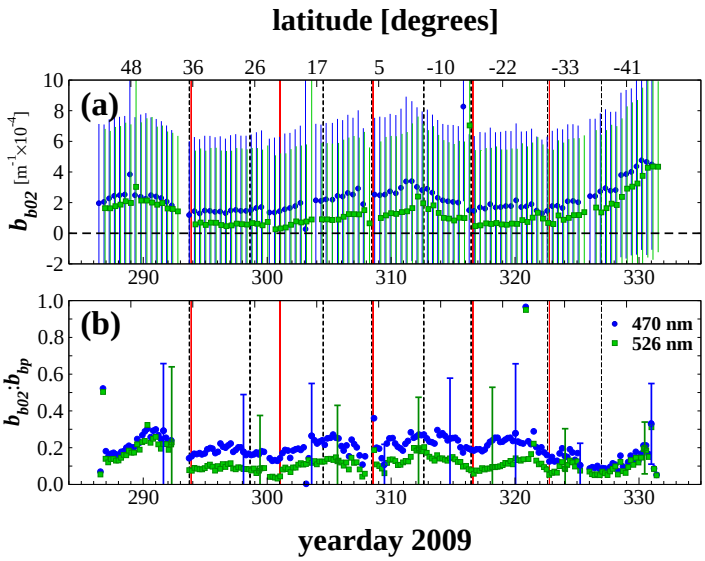

Fig. 8. Time series of **(a)** b_{b02} with error bars indicating 95% confidence intervals and **(b)** b_{b02}:b_{bp} with error bars representing standard errors plotted at discrete locations for clarity. Black dashed and red solid vertical lines indicate times when the flow-through system was cleaned and when the 0.2μm filter was replaced, respectively.

and recomputed the backscattering efficiency: (b_{bp}-b_{b02})/c_p. We found that (b_{bp}-b_{b02})/c_p was in good agreement with previous estimates of b_{bp}:c_p obtained using the same methodology (dashed line in Fig. 7(b)) and thus that most of the anomaly observed during AMT19 in the b_{bp}:c_p ratio was removed by subtracting b_{b02} from b_{bp}. One advantage of subtracting b_{b02} from b_{bp} is that any bias caused by uncertainties in dark counts and/or in $b_{b,wall}$ should cancel out. Thus, the improved agreement between (b_{bp}-b_{b02})/c_p and published values of b_{bp}:c_p supports the hypothesis that a bias of the same magnitude as the estimated uncertainties in b_b may affect our measurements.

Ancillary measurements would otherwise be needed to explain the real origin of b_{b02} and why it was higher during AMT19 than in other previous cruises in oligotrophic waters. Unfortunately these ancillary data (e.g., colloidal size distributions) were not collected. Some potential explanations are therefore discussed below.

If b_{b02} was indeed related to the presence of very small particles (i.e., colloids), it would seem reasonable to find a correlation between b_{b02} and the concentration of dissolved organic carbon (DOC). No measurements of DOC were available during AMT19, but some insights can be gained by comparing the spatial distributions of b_{b02} and existing DOC measurements. In general, DOC is relatively high in the tropical and subtropical surface ocean, where a stable mixed layer allows refractory DOC to accumulate [51]. On the other hand, DOC is lower at higher latitudes where the water column is less stable and DOC-depleted deep waters are mixed to the surface [51]. The observed b_{b02} values have a spatial distribution opposite to that expected for DOC, with higher values in the regions where the mixed layer was less stable (Fig. 8(a)). DOC, therefore, is unlikely to be the dominant control of b_{b02}, possibly because colloids are thought to contribute only 10% of DOC [52, 53].

Another potential explanation for the relatively high values of b_{b02} could be the presence of fine Saharan dust particles in the water. Dust deposition, however, is estimated to be one order of magnitude more intense in the northern than in the southern Atlantic (e.g., ref. [54]). If

#170689 - $15.00 USD Received 20 Jun 2012; revised 31 Aug 2012; accepted 31 Aug 2012; published 5 Sep 2012

atmospheric dust was responsible for the relatively elevated b_{b02} values, one would expect b_{b02} to be higher in the north than in the south Atlantic. Figure 8, however, does not show important differences in b_{b02} values between the northern and southern parts of the transect, suggesting that atmospheric dust is unlikely to be the cause of the elevated b_{b02}.

In conclusion, the b_{b02} measurements were anomalously higher than in previous cruises in meso- and oligotrophic regions, accounted for about 10% of the b_{bp} signal at 526 nm, and could explain the observed anomalies in the b_{bp}:c_p ratio. However, based on the available data, no clear biogeochemical explanation can be provided for this anomaly. It therefore seems most plausible that the b_{b02} values could be due to a bias of about 1×10^{-4} m^{-1} in our $b_{bp}(526)$ determinations. Importantly, such bias is well within the uncertainties of $b_{bp}(526)$. If such a bias was indeed the cause of the observed anomalies in b_{bp}:c_p and b_{b02}, then we could conclude that the AMT19 dataset confirmed the previous finding that b_{bp}:c_p is remarkably constant in the surface open ocean.

4.4. Uncertainties in b_{bp} and b_{b02}

Particulate backscattering estimates in oligotrophic regions are extremely sensitive to measurement uncertainties [25]. In this study, the main source of b_{bp} error was the uncertainty in the scaling factors (S) (Table 4). These uncertainties in S, in turn, depend on the uncertainties in multiple variables including the spectral and angular weighting functions of the instrument, as well as the complex refractive index and size of the beads used in the dilution series [35]. The relatively strong dependency between the uncertainties in S and b_{bp}, as well as the sensitivity analysis to the dark counts described in the method section highlight the need for a detailed understanding, characterization, and validation of the the instrument(s) employed for the measurements and the importance of identifying, quantifying and minimizing all sources of uncertainty affecting b_{bp} [35]. In particular, future studies should strive to validate particulate backscattering estimates by comparing measurements collected using instruments that employ different calibration procedures [35, 43, 61]. It is noteworthy that a recent publication by WET Labs scientists [35] has re-evaluated the angular weighting function, W, of WET Labs ECO-BB meters and suggests that W is centered at 124 degrees (instead of 117 degrees) and it is significantly wider than what was previously reported [25]. Nevertheless, to be consistent with our previous studies and until independent verification of this new specification is provided, in this study we have chosen to maintain the "standard" W function [25].

Overall our results and the above considerations emphasize the difficulties in obtaining accurate particulate backscattering measurements in the open ocean with the current instrumentation. This limitation is likely biasing the development and validation of open-ocean remote-sensing algorithms and it is hampering progress in the understanding of the sources of b_{bp} and in the application of b_{bp} measurements to the study of ocean biology and biogeochemistry.

4.5. Spectral slopes of c_p and b_{bp}

Important qualitative differences in the spectral slopes of b_{bp} and c_p were observed in this study (Figs. 6, 9). Under the hypotheses described in the introduction, the spectral slope of c_p should, theoretically, be linearly related to the slope of particle size distribution (PSD). Thus, γ_{cp} should increase as small particles become relatively more abundant than large ones [6, 29, 30]. Similarly, spectral b_{bp} has also been used to estimate the parameters of the particle size distribution [33].

During AMT19, b_{bp} spectra followed expected patterns [32, 33]: γ_{bbp} increased from the most eutrophic regions, where large cells are abundant, to the most oligotrophic regions that are dominated by small cells (Fig. 6). In contrast, γ_{cp} was maximal in eutrophic regions and minimal in oligotrophic waters (Fig. 6). To account for this anomalous behavior in γ_{cp}, one or

#170689 - $15.00 USD Received 20 Jun 2012; revised 31 Aug 2012; accepted 31 Aug 2012; published 5 Sep 2012

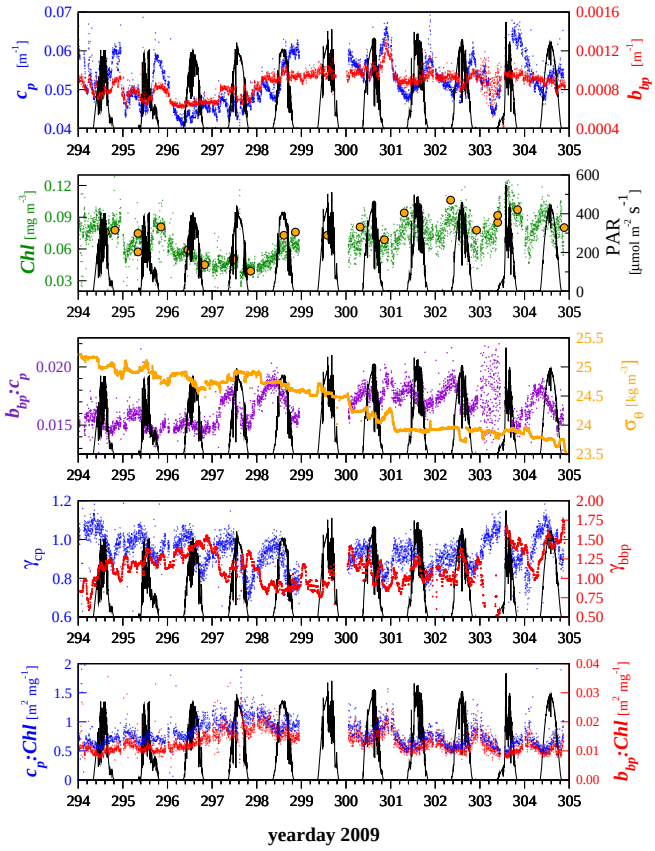

Fig. 9. Subset of time series showing diel cycles in each variable. Filled circles in the bottom plot are TChl-a estimates from discrete HPLC measurements. Values for γ_{bbp} were median filtered (window size of 120 minutes) to remove noise.

more of the above hypotheses must be invalid. Indeed, deviations from the power law approximation of the PSD are common in the open ocean, both in oligotrophic [32] and productive regions and have been shown to cause significant perturbations to γ_{cp} in coastal waters [56]. In addition, the acceptance angles of the AC9 and ACs transmissometers (0.93°) are known to reduce the instrument sensitivity to particles larger than about 10-20 μm [31].

During diel cycles, on the other hand, γ_{cp} followed expected dynamics, increasing during the day and decreasing at night (Figs. 6 and 9). These patterns have been previously observed [40,57,58] and are thought to be caused by the increase in size of synchronous cell populations during the day and their decrease at night following cell division [58,59].

4.6. Diel variability

Although spatial and temporal variability are superimposed in this dataset, diel cycles appeared to considerably affect the measured optical properties. As in previous studies [12, 40, 57, 58], these diel variations became most evident when the dependence on particle concentration was minimised by plotting ratios of optical properties (Fig. 6). b_{bp}:c_p, $b_p{}^*$, $b_{bp}{}^*$, γ_{cp}, and on closer inspection c_p, all showed diel variations, while b_{bp} and γ_{bbp} did not. *Chl* also showed clear diel

#170689 - $15.00 USD Received 20 Jun 2012; revised 31 Aug 2012; accepted 31 Aug 2012; published 5 Sep 2012

cycles, at least during some parts of the transect, decreasing during the day and increasing at night (Fig. 9). These diel cycles of *Chl* are confirmed by discrete HPLC measurements (Fig. 9). Diel cycles in optical properties are believed to be related to the dynamics of synchronized populations of phytoplankton cells (and associated living and non-living particles) [59,60]. Our dataset further demonstrates that this phenomenon is widespread in the surface Atlantic ocean.

5. Conclusions

An extensive data set of flow-through optical scattering properties collected in the surface Atlantic ocean was analyzed. The the main results are:

- The b_{bp}:c_p and b_{bp}:*Chl* ratios were higher than those predicted by existing bio-optical relationships and measured using the same methodology in other oceanic regions.
- b_{bp} from water filtered through 0.2 μm filters was higher than previous studies and contributed about 10% of the bulk $b_{bp}(526)$.
- The most parsimonious explanation for these anomalously high values of b_{bp} and b_{b02} is that a bias of the same order of magnitude of the measurement uncertainties (1×10^{-4} m^{-1} at 526 nm) affected our b_{bp} and b_{b02} measurements.
- If such bias indeed affected our b_{bp} measurements, then b_{bp}:c_p and b_{bp}:*Chl* ratios measured during AMT19 would be consistent with other global data sets and confirm the constancy of the b_{bp}:c_p ratio in surface open-ocean waters.
- These results emphasize the difficulties in obtaining accurate b_{bp} measurements in the oligotrophic open ocean.
- The spectral slopes of c_p and b_{bp} were found to be inversely correlated during the cruise, with γ_{bbp} following expected patterns.
- Diel cycles in all optical properties (except b_{bp} and γ_{bbp}) and bulk *Chl* were evident along the entire meridional transect, especially when ratios of properties were computed.

6. Appendix: Calibration of WET Labs ECO-BB3 meters

This section describes in detail the methodology employed to calibrate our BB3 meters for the AMT19 cruises and for our previous studies [8,12].

1. The BB3 meter, C-star transmissometer (660 nm) and flow-through chamber were thoroughly cleaned with Milli-Q water and a mild detergent and then thoroughly rinsed with Milli-Q water.
2. The BB3 was installed in the flow-through chamber and connected in series to the C-star transmissometer and to a 2L flask that was used as a reservoir.
3. A filter holder containing a 0.2-μm cartridge filter (Cole Parmer) was also installed in series in the above system.
4. The system was then filled with Milli-Q water. To minimize impurities in the system, the water was continuously recirculated through the 0.2-μm cartridge filter for about 1hr by means of an in-line pump.
5. The filter and filter holder were removed from the system.

#170689 - $15.00 USD Received 20 Jun 2012; revised 31 Aug 2012; accepted 31 Aug 2012; published 5 Sep 2012

6. With the pump switched off, data were recorded from both the BB3 meter and C-star transmissometer for about 1-2 minutes.

7. 1 or 2 drops of 2-μm NIST-traceable polystyrene beads (that had been sonicated for about 5 minutes; Thermo Scientific) were then added inside the reservoir and the pump was switched on to thoroughly mix the beads in the system, as verified by monitoring the data in real time. Note that WET Labs now recommends to use NIST-traceable 0.1-μm beads for channels at blue and green wavelengths [35], but this information was not available when the instruments used in this study were deployed. The use of 2-μm instead of 0.1-μm beads is expected to cause an underestimation of the scaling factors of about 5-10% (J. Sullivan, personal communication).

8. With the pump switched off, data were recorded from both the BB3 meter and C-star transmissometer for about 1-2 minutes.

9. The above two steps were repeated until the BB3 meter counts reached a value of 1000 (which was well above the counts encountered during AMT19).

10. Median values from the scattering data were linearly regressed vs. the median values of the BB3 counts at each dilution step to determine the slope of the relationship.

11. To compute the scaling factor $S(\theta,\lambda)$ the following equation was employed [25, 35]:

$$S(\theta,\lambda) = \left[\frac{\beta(\theta,\lambda)}{b_{\mathrm{AC9}}(\lambda)}\right]\left[\frac{Q_b^{\mathrm{AC9}}(\lambda)}{Q_b^{\mathrm{Cstar}}(650)}\right]\left[\frac{b_{\mathrm{Cstar}}(650)}{C(\lambda)}\right] \tag{4}$$

where:

- θ is the centroid angle of the BB3 (i.e., 117°). Note that a recent publication [35] suggests that the centroid angle of ECO-BB3 meters is now believed to be 124°. However, to be consistent with our previous studies [8, 12], we decided to adopt the 117° value until the new 124° value will be independently verified.

- λ is the wavelength (weighted by the spectral response of each instrument).

- $[\beta(\theta,\lambda)/b_{\mathrm{AC9}}(\lambda)]$ is a theoretical coefficient that relates the volume scattering function at the centroid angle and wavelength of the BB3 instrument to the scattering coefficient measured by a WET Labs AC9 meter at the same wavelength. This coefficient is computed through Mie simulations and depends on the characteristics of the beads (i.e., refractive index and size distribution) used, the spectral response and acceptance angle of the AC9, as well as on the the spectral responses and angular weighting function, W, of the BB3 meter (see definition of W and Eq. (9) in ref. [25]). Comparisons with the coefficients computed by WET Labs showed absolute differences of 4%, 9% and 1% in the 470, 526, and 656 nm channels, respectively. The larger difference in the green channel could be related to the shift from the nominal green wavelength that we observed [12]. Note also that WET Labs did not routinely employ NIST-traceable beads and that the difference in scaling factors estimated based on dilution series using NIST-traceable and non-NIST-traceable beads (of the same nominal size) can be up to 8% (J. Sullivan, personal communication).

- $[Q_b^{\mathrm{AC9}}(\lambda)/Q_b^{\mathrm{Cstar}}(650)]$ is a theoretical coefficient used to convert C-star scattering measurements into equivalent AC9 scattering measurements. $Q_b^{\mathrm{AC9}}(\lambda)$ and $Q_b^{\mathrm{Cstar}}(650)$ are the efficiency factors for scattering. We derived these coefficients by means of Mie

#170689 - $15.00 USD Received 20 Jun 2012; revised 31 Aug 2012; accepted 31 Aug 2012; published 5 Sep 2012

simulations that accounted for the characteristics of the beads employed and the spectral responses and acceptance angles of the two instruments.

- $[b_{\mathrm{Cstar}}(650)/C(\lambda)]$ is the experimental slope computed by linearly regressing median C-star measurements, $b_{\mathrm{Cstar}}(650)$, versus the median counts recorded by the BB3 instrument at each wavelength, $C(\lambda)$, and at each bead dilution step.

Acknowledgements

The authors would like to thank the captain and crew members of the *RSS James Cook*. C. Gallienne is thanked for his help in deploying the profiling package. J. Sullivan at WET Labs and an anonymous reviewer are thanked for their comments on an earlier draft of this manuscript. G.D.O. was funded by NASA grant NNX09AK30G and by the UK National Centre for Earth Observations. This study was supported by the UK Natural Environment Research Council National Capability funding to Plymouth Marine Laboratory and the National Oceanography Centre, Southampton. This is contribution number 218 of the AMT programme.

#170689 - $15.00 USD Received 20 Jun 2012; revised 31 Aug 2012; accepted 31 Aug 2012; published 5 Sep 2012